

CrossMark
click for updatesCite this: *RSC Adv.*, 2016, 6, 61585

Novel biotin-functionalized lipidic nanocarriers for encapsulating BpT and Bp4eT iron chelators: evaluation of potential anti-tumour efficacy by *in vitro*, *in vivo* and pharmacokinetic studies in A549 mice models†

Shweta Dumoga,^{ab} Namit Dey,^a Anivind Kaur,^a Surendra Singh,^b Anil K. Mishra^{*a} and Dipti Kakkar^{*a}

Tumour cells have a high demand for iron (Fe) due to their rapid rate of proliferation. Strategies to target intracellular iron for antitumour therapy have not been systematically explored. The benzoylpyridine thiosemicarbazone (BpT) group of Fe-binding drugs represent a promising class of anti-tumour agents; however, their low aqueous solubility and high protein binding limit their clinical efficacy. In this work, we have explored the possibility of using solid lipid nanoparticles (SLNs) to develop a nanocarrier system that can deliver a drug cargo of BpT drugs to tumour sites. Herein, we prepared targeted biotinylated stearic acid based PEGylated SLN formulations for entrapment of benzoylpyridine thiosemicarbazone (BpT) and its analogue 4-ethyl benzoylpyridine thiosemicarbazone (Bp4eT) by the ultrasonication method, resulting in BpT-PB-SLNs and Bp4eT-PB-SLNs (size 115 to 120 nm, zeta potential -28 to -36 mV) with EEs of 72%. These formulations had negligible hemolytic activity and sustained drug release for 7 days. Radiolabeling with technetium-99m (^{99m}Tc) radionuclide facilitated the evaluation of their biological parameters both *ex vivo* and *in vivo*. Their blood kinetics profile showed prolonged systemic circulation compared to native drugs (BpT and Bp4eT) in New Zealand albino rabbits. The biodistribution studies performed in A-549 xenografted athymic mice depicted higher tumour uptake and lower non-specific uptake than native drugs as confirmed through whole body SPECT imaging by semi-quantitative analysis. This research presents for the first time a novel lipidic nanocarrier system in the form of biotin functionalised PEGylated SLNs that can help deliver iron chelators in a highly sustained manner and therefore hold potential to enhance their intracellular uptake and hence their antitumour efficacy.

Received 2nd February 2016
Accepted 25th May 2016

DOI: 10.1039/c6ra03079c

www.rsc.org/advances

Introduction

The inability of conventional chemotherapeutics to efficiently distinguish between malignant and healthy cells has tremendously increased the need for highly specific and novel cures for affected cells. Nanocarriers have vast potential for improvising the therapeutic index of drugs by stabilizing and protecting drugs, improving their solubility and reducing their non-specific uptake by the reticuloendothelium system (RES).¹ The

aspect of selective targeting is currently still a formidable challenge; however, linking nanocarriers with specific ligands that bind to receptors or molecules overexpressed on tumour cell surfaces are among the most promising approaches being utilized to confront the same.² Ligands such as folic acid, biotin, transferrin, and epidermal growth factor, which target folate receptors, lecithins (through avidin), transferrin receptors and epidermal growth receptors on tumour cells, can guide nanocarriers specifically towards cancer cells.³ Chemotherapy, which once appeared to be the only viable approach towards anti-cancer treatment, is now gradually being substituted with alternative, less toxic approaches such as immunotherapy, gene therapy, radiation therapy, and antibody-mediated drug treatment.^{4,5} One such strategy involves depriving the growing cancer cells of essential nutrients to limit their uncontrolled proliferation. Iron is a vital cofactor for several proteins and enzymes and plays a crucial role in cell cycle regulation, cellular metabolism and cell division, which explains its higher requirement by neoplastic cells.⁶ Overexpression of transferrin

^aInstitute of Nuclear Medicine and Allied Sciences, Brig. S. K. Mazumdar Road, Timarpur, Delhi-110054. E-mail: akmishra@inmas.drdo.in; dipti@inmas.drdo.in

^bDepartment of Chemistry, University of Delhi, Delhi-110007

† Electronic supplementary information (ESI) available: Scheme for synthesis of BpT and Bp4eT (Scheme S1), characterization of BpT and Bp4eT by ^1H and ^{13}C NMR, mass, IR and UV/Vis spectroscopies (Fig. S1–S5), calibration curves of BpT and Bp4eT in acetate buffer (pH 5.5) and PBS (pH 7.4, 0.1 M) (Fig. S6), model fitting for drug release kinetics (Fig. S7), quality control of radiolabelled compounds (Fig. S8), *in vitro* serum stability (Fig. S9), biodistribution profile of BpT and Bp4eT (Fig. S10). See DOI: 10.1039/c6ra03079c

receptors on tumour cells further validates the enhanced iron requirement theory, as these receptors are involved in intracellular iron transport.⁷ By leveraging this fact, significant cellular changes can be expected when tumour cells are starved of iron and subjected to reduced levels of intracellular iron. Keeping in mind the perceived increased dependence of cancerous cells on iron, it would not be inappropriate to employ the concept of cellular iron depletion through chelation as a possible therapeutic intercession in different types of cancers. Iron chelators have been explored as cancer chemopreventive and chemotherapeutic agents through the depletion of intracellular iron.

The chemopreventive and chemotherapeutic efficacy of iron chelators has already been demonstrated in a wide range of studies on aggressive tumours, such as cytotoxic drug-resistant lung carcinoma M109 cells and MBT and T24 bladder cancer cells.^{8,9} These include chelators such as hexadentate siderophores, desferrioxamine (DFO),¹⁰ tachpyridine,¹¹ the aroylhydrazine class of chelators (such as the pyridoxal isonicotinoyl hydrazine series, PIH, and its analogues),¹² the thiohydrazine series, and the thiosemicarbazone class of chelators (DpT series and BpT series).^{13,14} Among these, the thiosemicarbazones, namely di-2-pyridylketonethiosemicarbazone (DpT series) and 2-benzoylpyridine thiosemicarbazone (BpT series, formed by replacing the 2-pyridyl ring of DpT with a phenyl group) combine critical structural features that are necessary to confer potent anti-proliferative effects. Richardson and co-workers have reported greater anti-proliferative activity for the novel BpT chelators, perhaps resulting from an increased electron-withdrawing effect from the pyridyl nitrogen, essential for Fe-binding affinity.¹⁵ Clinical trials have demonstrated the anti-proliferative potential of iron chelators such as DFO for patients with neuroblastoma¹⁶ and thiosemicarbazones such as 3-aminopyridine-2-carboxaldehyde thiosemicarbazone (Triapine®; Vion Pharmaceuticals Inc., New Haven, CT) in phase I and II clinical trials of patients with metastatic renal cell carcinoma and advanced pancreatic adenocarcinoma.¹⁷

However, these anti-tumour effects have been associated with some adverse effects, such as dose-limiting toxicity (including anaemia, leucopenia, methaemoglobinemia, thrombocytopenia and hemolysis), which have been observed in clinical trials of 3-aminopyridine-2-carboxaldehyde thiosemicarbazone (Triapine), while cardiac fibrosis has been reported with di-2-pyridylketone-4,4-dimethyl-3-thiosemicarbazone (Dp44mT) of the DpT series.^{18,19} Moreover, the low aqueous solubility of these iron chelators further decreases the scope of their potential use as injectable formulations. Additionally, studies have shown the high protein binding of the BpT class of compounds, which has been further reported to reduce cellular uptake and apoptotic activity and therefore compromise the anti-proliferative activity of these compounds.²⁰ Pharmacokinetics studies in rats have found Bp4eT and its metabolites in plasma 2 h after administration and in urine 24 h after administration, indicating that some fraction of administered Bp4eT is eliminated unchanged from *in vivo* systems.^{21–24} These impediments to the chemical efficacy of these compounds, if addressed, could greatly help the further clinical development of iron chelators. The encapsulation

of drugs is one such technique, involving the use of nanotechnology based drug carriers to offer potentially improved strategies/methodologies to overcome the drawbacks of native drugs.²⁵ Further PEGylation of these nanocarriers not only helps to improve the solubility of water-insoluble drugs but also prolongs their circulation in the blood by providing stealth characteristics.²⁶ To our knowledge, limited literature is available on iron-chelator encapsulated nanoparticulate carriers, especially for chemotherapeutic applications. There are only a few reports on liposomal and micellar formulations encapsulating iron chelators; also, these have been used for iron overload disorders, such as β -thalassemia.^{27,28} Miao *et al.* reported a hyperbranched copolymer system to encapsulate Bp4eT and examined its intracellular delivery in HepG2 and H1299 cells.²⁹ Recently, Mir *et al.* reported the preparation of deferasirox loaded polymeric nanoparticles.³⁰ Nonetheless, solid lipid nanoparticles (SLNs), a highly bio-compatible nanoparticulate carrier system, does not appear to have been explored at all for the delivery of iron chelators, especially for chemotherapeutic applications.³¹ The present investigation is the first to demonstrate a novel strategy to use targeted SLNs to encapsulate BpT and its analogue Bp4eT and validate the chemotherapeutic potential of this system.

We have developed a stearic acid based PEGylated solid lipid nanoparticle formulation (with biotin as the targeting ligand) to encapsulate the potential anti-proliferative agents BpT and Bp4eT and deliver them to the tumour site, thus offering an opportunity to overcome issues with these native drugs. These targeted PEGylated SLNs were prepared by the ultrasonication method and targeted to tumour tissues using biotin as a targeting ligand. This work presents a two-step pre-targeting approach to target tumours by exploiting the extremely high binding affinity of biotin to the avidin protein. This paper describes detailed *in vitro* and *in vivo* studies to evaluate the cytotoxicity, serum stability and hemolytic activity of these formulations to give more insights into their anti-proliferative activity. To evaluate further, both native drugs (BpT and Bp4eT) and drug loaded targeted SLNs have been radiolabelled with a gamma nuclide, technetium-99m (^{99m}Tc), to investigate their pharmacokinetics and pharmacodynamics by studying their blood kinetics in rabbits, biodistribution in A549 tumour models and uptake in tumour tissues. These pharmacokinetics studies have been further confirmed by scintigraphic imaging in A549 xenografted nude mice.

Experimental

Materials and methods

2-Benzoylpyridine, thiosemicarbazide and 4-ethyl-3-thiosemicarbazide were procured from Sigma Aldrich. Ethanol, HPLC-grade water, glacial acetic acid and diethyl ether were bought from E-Merck Co. Ltd. Stannous chloride dehydrate, Tween-80, biotin, avidin and human serum albumin (HSA) were procured from Sigma Aldrich, USA. Stearic acid (SA), soya lecithin and Triton X-100 were procured from CDH Fine Chemicals, Delhi, India. ^{99m}Tc was obtained in the form of its sodium salt, [Na^{99m}TcO₄], eluted from a ⁹⁹Mo/^{99m}Tc generator

by a solvent extraction method, as supplied by the Regional Center for Radiopharmaceuticals (northern region), Board of Radiation and Isotope Technology (BRIT) (unit of BARC), Department of Atomic Energy, India. Human NSCLC cell line A549 was purchased from American Type Culture Collection (Rockville, MD, USA).

Animal models

Healthy athymic mice (weighing between 20 and 25 g) and albino New Zealand rabbits with body weights between 2.5 and 3 kg and with no prior drug treatment were used for the blood kinetics, imaging and biodistribution studies. All animal studies were carried out in accordance with the guidelines compiled by CPCSEA (Committee for the Purpose of Control and Supervision of Experiments on Animals), Ministry of Culture, Govt. of India, and all the study protocols were first approved by the Institutional Animal Ethics Committee. Mice and rabbits were housed at the in-house Experimental Animal facility, under controlled temperature conditions of $22\text{ }^{\circ}\text{C} \pm 2\text{ }^{\circ}\text{C}$, and were kept on a standard diet and water. All possible steps were taken to abate the suffering of the animals at each stage of the experiment.

A549 xenografts. A549 cells were maintained in RPM1 medium supplemented with 10% (v/v) heat inactivated fetal bovine serum, 2 mM L-glutamine and 100 U mL^{-1} penicillin-streptomycin in a humidified incubator at $37\text{ }^{\circ}\text{C}$ in 5% CO_2 . $100\text{ }\mu\text{L}$ PBS containing 2×10^6 A549 cells were subcutaneously injected into the right flank of the athymic mice. After 7 to 10 weeks, the tumour volumes reached around 50 mm^3 and the mice models were ready for biodistribution and imaging studies.

Synthesis

Synthesis of 2-benzoyl pyridine thiosemicarbazone (BpT). 2-Benzoyl pyridine thiosemicarbazone (BpT) was synthesized according to a protocol by Richardson *et al.*, with slight modifications, using Schiff-base condensation.³² 2-Benzoyl pyridine (2.0102 g, 10.972 mmol) was dissolved in EtOH (20 mL). $80\text{ }\mu\text{L}$ of glacial acetic acid was added to a 5% aqueous solution of thiosemicarbazide (1 g, 10.972 mmol) and refluxed for 8 to 10 h. The mixture was cooled to $5\text{ }^{\circ}\text{C}$ and the yellow precipitate formed was washed with a 1 : 1 mixture of EtOH : acetone followed by washing thrice with diethyl ether to obtain BpT in the form of yellow crystals (yield: $\sim 70\%$).

Synthesis of 2-benzoylpyridine-4-ethyl-3-thiosemicarbazone (Bp4eT). The synthesis of 2-benzoyl pyridine 4-ethyl-3-thiosemicarbazone was performed by the same method as BpT, by using 4-ethyl-3-thiosemicarbazide (500 mg, 4.19 mmol) in place of thiosemicarbazide along with 2-benzoyl pyridine (768.5 mg, 4.19 mmol). Similar processing resulted in pale yellow shiny crystals of Bp4eT (yield: $\sim 72\%$).

Synthesis of PEG-biotin conjugate (PB). The PEG-biotin conjugate was prepared by Steglich esterification.³³ In brief, methoxy-PEG₅₀₀₀ (341.1 mg, 0.068 mmol) was dissolved in DMF (15 mL). A solution of biotin (20 mg, 0.0818 mmol), DCC (35.18 mg, 0.1704 mmol) and DMAP (8.33 mg, 0.068 mmol) in DMF (15

mL) was added dropwise to the methoxy-PEG₅₀₀₀ solution. After stirring for 72 h at room temperature, the reaction mixture was concentrated and the product was precipitated in 20 mL of cold diethyl ether and further purified by washing thrice with diethyl ether. PEG-biotin was obtained as a light brown powder (yield: $\sim 95\%$).

Chemical characterization

Nuclear magnetic resonance. ^1H NMR and ^{13}C NMR analysis was performed on a Bruker Avance 400 MHz spectrometer in 5 mm diameter WILMAD® NMR tubes. 10 to 20 mg of the compound was dissolved in $700\text{ }\mu\text{L}$ CDCl_3 for evaluation.

Infrared spectroscopy. Functional groups were analyzed using a Thermo Scientific Nicolet 8700 ATR instrument.

Mass spectroscopy. ESI mass spectra were recorded on an Agilent Technologies 6310 Ion-Trap LCMS.

UV-Vis spectroscopy. UV-Vis spectra were recorded on a Synergy 2 Multi-mode reader by BioTek Instruments, Inc., USA.

Nanoparticle formation of BpT and Bp4eT loaded PEGylated solid lipid nanoparticles (SLNs)

Stearic acid based solid lipid nanoparticles (SLNs) were previously optimized by our group, and the optimal formulation in terms of size and polydispersity index (PDI) was used for loading these iron chelators.³⁴ In this work, the synthesized PEG-biotin was incorporated in the SLN formulation instead of the PEG used earlier. Briefly, stearic acid was heated to $50\text{ }^{\circ}\text{C}$ (in a water bath) and added to the organic phase comprising a 1 : 1 mixture of acetone and ethanol. An aqueous phase containing the surfactant Tween-80 and the co-surfactant soya lecithin in a 1 : 1 ratio was maintained at pH 1.1 with 1 N HCl in an ice bath. The hot organic phase was quenched by pouring it into the aqueous phase, maintained at $0\text{ }^{\circ}\text{C}$, under constant stirring. The resulting o/w emulsion was further sonicated in a bath sonicator (Bandelin Sonorex RK52H, Germany) for 15 min and a probe sonicator (VCX 750, Vibracell™, Sonics & Materials Inc., Newton CT, USA) for 5 min. The SLNs dispersions were purified by centrifugation at $4\text{ }^{\circ}\text{C}$ (Eppendorf 5810R Centrifuge, Thermo Fisher Scientific, USA) at 10 000 rpm, followed by water washings ($\times 3$) until the supernatant was completely neutral (pH 7.0). The resulting formulation had the following composition (w/v%): lipid 1.1%, PEG-biotin 0.125%, soya lecithin 2.5% and Tween-80 2.5%. The drug loaded SLNs were similarly prepared by adding BpT and Bp4eT drugs (0.1 to 1.1%) to the formulation. These formulations were hence named BpT-PB-SLNs and Bp4eT-PB-SLNs for BpT and Bp4eT loaded SLNs, respectively. The SLN suspensions were lyophilized in a freeze-drier to obtain them in dry powder form for further evaluation (Freezone 2.5 plus, Labconco Corporation, MO, USA).

Physico-chemical characterization

Dynamic light scattering and zeta potential. The dry powder of the SLN formulation was re-suspended in water to form a homogenous solution. This solution was used for the determination of the hydrodynamic diameter and zeta potential

measurements using the dynamic light scattering technique (Malvern Zetasizer 90S, UK). All the measurements were performed in triplicate.

Transmission electron microscopy and atomic force microscopy. The morphology of BpT-PB-SLNS and Bp4eT-PB-SLNS was analyzed by TEM (HITACHI, H-7500, Japan). One drop of the loaded SLN formulation was placed on a carbon coated copper grid of 200 mesh size and air dried to evaluate the morphology by TEM. AFM microscopy (ScanAsyst®, Bruker, USA) was also used to support the TEM images. Samples were prepared by spraying the aqueous formulations onto silicon wafers and air-drying them.

Determination of drug content in the SLNs

The entrapment efficiency (% EE) and drug loading (% DL) of BpT-PB-SLNs and Bp4eT-PB-SLNs was determined by disrupting the drug-loaded SLNs in DMSO (1 mg mL⁻¹). The drug content dissolved in DMSO was determined using UV-spectroscopy at 330 nm. The % EE and % DL were calculated as follows:

$$\text{Drug loading (\% DL)} = \frac{\text{amount of drug encapsulated in SLNs}}{\text{amount of drug added}} \times 100$$

$$\text{Entrapment efficiency (\% EE)} = \frac{\text{amount of drug encapsulated in SLNs}}{\text{amount of SLNs}} \times 100$$

Drug release profile and kinetics

The dialysis method was used to study the release of the drugs (BpT and Bp4eT) from the iron chelator loaded PEGylated SLNs. To quantify their release, suspensions of BpT-PB-SLNs and Bp4eT-PB-SLNs in PBS (pH 7.4) were analyzed by UV-Vis spectrophotometry. For comparison, the BpT and Bp4eT released from the solution were also analyzed under similar conditions. All the experiments were performed in triplicate from the same stock solutions. The release studies were examined at two different pH values, 7.4 (0.1 M phosphate buffer saline) and 5.5 (acetate buffer), using a Spectra-Por® Float-A-Lyzer (MWCO 8 kDa, Spectrum Laboratories, USA). The Float-A-Lyzer was soaked overnight in distilled water. 5 mL of each drug loaded nanocarrier was transferred to the Float-A-Lyzer, which was then placed in the respective buffer solution (dialysis medium). 2 mL aliquot was withdrawn from the dialysis medium to record its UV absorbance and was refurbished with 2 mL of fresh buffer. Calibration curves of BpT and Bp4eT in acetate buffer and PBS were used to calculate the drug concentration in the SLNs (Fig. S2†). The following equation was used to calculate the cumulative percentage of drug released from the SLNs:

$$\% \text{ drug release} = \left[1 - \left\{ \frac{\text{absorbance}_t}{\text{absorbance}_{t_0}} \right\} \right] \times 100$$

The absorbance was measured at time t_0 (initial time) and at time t .

To further evaluate the mechanism of drug release from the nanocarriers, the release data was plotted according to different kinetic models (zero order ($M_t = K_0t$), first order ($\log M_t = K_1t$), Higuchi model ($M_t = K_h t^{1/2}$) and Korsmeyer-Peppas model ($\frac{M_t}{M_\infty} = K_{kp} t^n$), where M_t and M_∞ are the drug released at time, t and at infinite time respectively, K_h is the Higuchi dissolution constant and K_{kp} is the drug release rate constant).

In vitro evaluation

Hemolysis studies. Interaction of BpT-PB-SLNs and Bp4eT-PB-SLNs with red blood cells (RBCs)/erythrocytes was examined by hemolysis studies. The hemolytic activity of the native drugs (BpT and Bp4eT) and the drug loaded targeted SLNs was evaluated in accordance with ASTM F756 as per protocol.³⁵ Briefly, blood was drawn from healthy human volunteers in heparinized tubes and then centrifuged at 3000 rpm for 10 min to separate the RBCs from the plasma. The RBC pellet was washed thrice with PBS (pH 7.4) and suspended in 50 mL of PBS 7.4 to form a RBC suspension. In each case, 0.4 mL of sample (BpT and Bp4eT solution and BpT-PB-SLNs and Bp4eT-PB-SLNs dispersion with equivalent drug concentration) was mixed with 1.6 mL of the RBC suspension. These were incubated after gentle mixing at 37 °C to evaluate the time dependent hemolytic character of the compound. At different time points ranging from 15 min to 4 h, 2 mL of the mixture was centrifuged for 10 min at 3000 rpm to precipitate the erythrocytes. The optical density of the supernatant was measured at 540 nm using a UV-Vis spectrophotometer, and the (%) hemolysis was calculated using the following formula:

$$\% \text{ hemolysis} = \frac{\text{absorbance}_{(\text{compound})} - \text{absorbance}_{(-\text{ve control})}}{\text{absorbance}_{(+\text{ve control})} - \text{absorbance}_{(-\text{ve control})}} \times 100$$

Methemoglobin formation. RBC pellets prepared as describe above were lysed with ultra-pure water; the remaining debris was separated by centrifugation at 14 000g for 30 min at 4 °C. The supernatant which contained the RBC lysates was used for further experiments. The concentration of MethHb in the RBS lysates was evaluated to be 630 nm by UV-Vis spectrophotometry.³⁶ Chelators (BpT, Bp4eT and DFO)-iron complexes were freshly prepared by combining the ligand with FeCl₃·6H₂O in DMSO (2 : 1 = ligand : metal), the most stable form of the complex.³⁷ The BpT-Fe and Bp4eT-Fe complexes were further encapsulated in SLNs as per the abovementioned protocol. The chelator-iron complexes were all used in equal concentrations (25 μM). All the complexes were incubated with both intact RBCs and RBC lysates for 4 h at 37 °C to evaluate the methemoglobin formation compared with that of the DFO-Fe complex, which is not redox-active.

Sulforhodamine B assay. A sulforhodamine B (SRB) assay was carried out to determine the cytotoxicity of BpT and Bp4eT loaded SLNs in human embryonic kidney cells (HEK). Cells were

seeded into 96-well plates (2000 to 5000 per well), allowed to attach overnight, and then incubated with 0.01 to 100 μM BpT, Bp4eT and their encapsulated SLNs, respectively. The media was removed at defined time points of 12, 24 and 48 h and 100 μL of 10% trichloroacetic acid (TCA) was added to the wells at 4 $^{\circ}\text{C}$ to precipitate the proteins. After 45 min of incubation, the unbound TCA was removed by the addition of 200 μL of deionized water followed by the addition of 100 μL of 0.4% SRB solution to each well and incubated at 37 $^{\circ}\text{C}$ for 30 minutes. The SRB from each well was washed a minimum of 5 times with 1% acetic acid solution and then air dried. The protein bound dye was then solubilized by adding 100 μL of 10 mM Tris base to each well for 30 minutes at 37 $^{\circ}\text{C}$. The final step of the protocol involved a homogenisation step by placing the plate on a shaker for 10 minutes, followed by measuring its absorbance at 564 nm using a UV-Vis spectrophotometer.

$$\text{Percentage viability} = \left[\frac{\text{OD}_{\text{compound}}}{\text{OD}_{\text{control}}} \right] \times 100$$

Radiolabeling and *in vivo* evaluation

The drug-loaded and unloaded formulations were labeled with $^{99\text{m}}\text{Tc}$ radionuclide using the previously used labeling method with slight modifications.³⁸ In short, the fresh solution of sodium pertechnetate in saline (74 to 110 MBq of $^{99\text{m}}\text{TcO}_4^-$) was added to each formulation, followed by addition of stannous chloride solution (reducing agent for pertechnetate) in 10% glacial acetic acid (4 mg mL^{-1}). The acidic pH was neutralized by adding 0.1 M NaOH solution. The labeling efficiency of the nanoformulations was examined using instant thin layer chromatography (ITLC) in different solvent systems (acetone and PAW (pyridine : acetic acid : water: 3 : 5 : 1.5)) as per the literature, to evaluate the percentage of $^{99\text{m}}\text{Tc}$ labeled formulation in the mixture with regard to the reduced and hydrolyzed colloids formed.³⁹

Blood kinetics

For the blood kinetics studies of $^{99\text{m}}\text{Tc}$ -labeled SLNs and $^{99\text{m}}\text{Tc}$ -labeled drugs, healthy New Zealand albino rabbits weighing 2.5 to 3.5 kg were used. 300 μL (10 MBq) of each $^{99\text{m}}\text{Tc}$ labeled SLNs formulation was injected in the dorsal ear vein. Blood was drawn from the other ear vein at different time intervals ranging from 5 min to 24 h, to evaluate the continuous activity of these formulations in the blood circulation. The percentage of the injected dose remaining in blood was calculated for each time interval, assuming a total blood volume equal to 7% of body weight.

***In vitro* serum stability.** The above blood samples were used to separate the plasma by centrifugation. To this, 10% TCA was added to separate the plasma proteins. $^{99\text{m}}\text{Tc}$ labeled SLNs and iron chelators were incubated with the remaining serum at 37 $^{\circ}\text{C}$, and their stability was evaluated after 24 h incubation by measuring their respective radioactivities in a well-type gamma counter.

Biodistribution

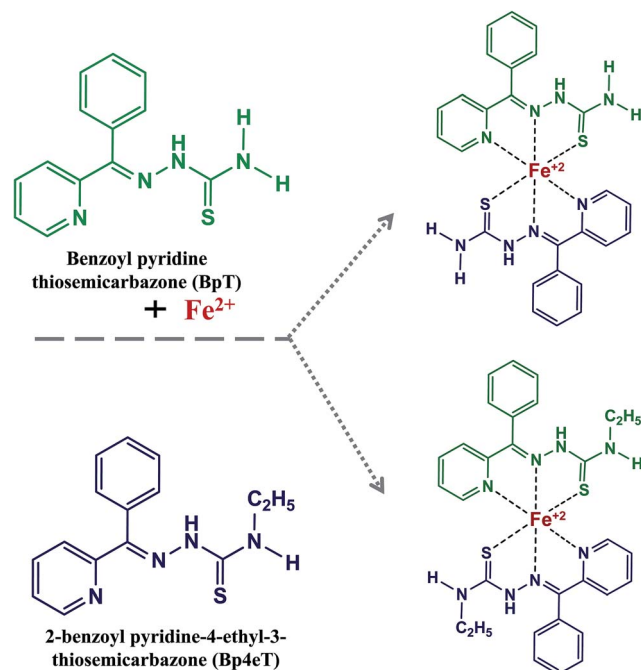
A549 xenografted athymic (nude) mice were divided into two groups of twelve each. 100 μL (3.7 MBq) of $^{99\text{m}}\text{Tc}$ labeled SLNs formulations were introduced in the tail vein of the xenografted mice. Prior to this, the mice were injected with avidin. At different time intervals (1 h, 2 h, 4 h and 24 h), the mice ($n = 3$) were euthanized and blood was collected into pre-weighed vials. The nude mice were then dissected and their vital organs (lungs, heart, liver, kidneys, spleen, stomach, intestine, tumour muscle and contralateral muscle) were removed. The organs were washed with saline to remove any debris and collected in pre-weighed vials. The radioactivities of these organs were measured by a gamma counter. The measurement of remnant radioactivity in each organ was calculated per gram organ weight and conveyed as the % injected dose per gram organ weight. The radioactivity of the tail (point of injection) was also measured to evaluate the absolute percentage of remaining radioactivity in a particular organ.

SPECT imaging

To further evaluate the tumour specificity of these biotin functionalized SLNs, a competitive binding study was performed by pre-targeting the tumour bearing mice with avidin at least 2 h prior to injection. Six A549 xenografted (nude) mice were co-injected with 100 μL each of unlabeled biotin, $^{99\text{m}}\text{Tc}$ labeled BpT-PB-SLNs and $^{99\text{m}}\text{Tc}$ Bp4eT-PB-SLNs (3.7 MBq) (three mice for each compound). Gamma images were captured using a HAWK-EYE gamma camera attached with a collimator. Semiquantitative analysis was performed using INTEGRA Software by generating a region of interest (ROI) to evaluate the uptake of nanoformulations in the tumour region.

Results and discussion

Rapidly dividing cancer cells have a higher requirement for iron than their normal counterparts, making them sensitive to iron depletion. The current research is based on the hypothesis that iron depletion strategies may have deleterious effects on tumour cell growth and may be possible solutions to counter it.¹⁵ The 2-benzoyl thiosemicarbazone series of iron chelators have shown promising anti-tumour effects, but with scope for improvement with regard to their associated drawbacks. Therefore, the aim of this work is to develop a functionalized SLN carrier system for the BpT and Bp4eT iron chelators so as to enhance their antiproliferative effects and overcome the drawbacks of the native drugs. This work elaborates the synthesis of these two chelators, BpT and Bp4eT, and their entrapment in SLNs (Schemes 1 and S1 of the ESI[†]). PEG-biotin conjugate has been incorporated in these solid lipid NPs to serve a dual purpose (Fig. S6[†]). The dense poly(ethylene glycol) shell of the SLNs can prevent protein adsorption and recognition by the phagocyte system and prolong blood circulation, a prerequisite for enhanced tumour accumulation based on the EPR effect.⁴⁰ Biotin is being used as a ligand to target tumours by a two-step pre-targeting approach, leveraging its high specificity and strong affinity ($K_d = 10^{-15}$ M) to avidin. Avidin (a highly



Scheme 1 Bidentate ligands, benzoyl pyridine thiosemicarbazone (BpT) and 4-ethyl benzoyl pyridine thiosemicarbazone (Bp4eT) showing Fe^{2+} chelation.

glycosylated, positively charged protein found in egg white) binds to lectins (proteins that bind to the cell membranes) which are expressed at various levels on the surface of tumour cells.^{41,42} The biotin–avidin interaction, considered a gold standard for the two-step pretargeting approach to tumour sites, has shown good results in these iron chelator loaded SLNs to help deliver the iron chelators inside the tumour cells. Moreover, the tetrameric architecture of avidin (fourfold valency for biotin) offers amplified accumulation of the targeted formulations at the tumour site. This has been extensively studied with the help of radiolabeling techniques. In our study, we have used a gamma emitter, ^{99m}Tc, which is a metastable nuclide with an optimal half-life ($t_{1/2} \sim 6$ h) for evaluation yet low radiation exposure to the subject. The BpT and Bp4eT encapsulated biotinylated SLNs thus developed/prepared were evaluated by physico-chemical characterization techniques followed by their *in vitro*, *ex vivo*, and *in vivo* evaluation in A549 tumour models.

Synthesis – chemical characterization

2-Benzoylpyridine thiosemicarbazone was synthesized by a Schiff-base condensation reaction between 2-benzoylpyridine and thiosemicarbazide, as shown in Scheme S1.[†] Similarly, Bp4eT, an analogue of BpT, was synthesized by the same protocol using 2-benzoylpyridine and 4-ethyl-3-thiosemicarbazide. The Bp4eT analogue was prepared by replacing one H attached to N with an ethyl group ($-\text{CH}_2-\text{CH}_3$). This functionalization would cause an increase in the +R effect and the electron-donating effect of the chelator and would therefore result in stronger metal binding than BpT. The

products, BpT and Bp4eT, were characterized by ¹H NMR, ¹³C NMR, FTIR, and ESI-MS and UV-Vis spectroscopies. The ¹H NMR spectra of both of the drugs depicted all the peaks of their respective protons, while the ¹³C spectra showed the disappearance of the carbonyl peak of 2-benzoylpyridine at 193.79 ppm and the appearance of the imine peak of BpT at 152.22 ppm and at 152.40 ppm in the case of Bp4eT (Fig. S1 and S2[†]). The mass spectrum for BpT showed a $[\text{M} + \text{H}]^{+1}$ peak at 257.3 *m/z*, while the $[\text{M} + \text{Na}]^{+1}$ peak appeared at 279.1 *m/z*. The Bp4eT spectrum showed a $[\text{M} + \text{H}]^{+1}$ peak at 285.3, while the $[\text{M} + \text{Na}]^{+1}$ peak appeared at 307.0 *m/z* (Fig. S3[†]). This was also corroborated by the qualitative FTIR spectra with the disappearance of the carbonyl stretching at 1666 cm^{-1} (corresponding to 2-benzoylpyridine) and the appearance of $\nu_{\text{C}=\text{N}}$ stretching at 1592 cm^{-1} (corresponding to the imine) (Fig. S4[†]). The synthesis was evident from the shift in the λ_{max} values obtained from the UV-Vis spectra (Fig. S5[†]).

Nanoparticle formation – characterization and drug loading

Here, we attempted to incorporate the synthesized iron chelators BpT and Bp4eT in a biocompatible lipidic carrier system to help deliver them in higher concentrations at the target tumour site with minimum wastage due to protein binding, *etc.*, *en route*. In addition, this work also aimed to compare the behaviour of these two drugs when they are encapsulated in a functionalized PEGylated lipidic carrier system with biotin as the targeting ligand to increase the tumour targeting efficacy.⁴³ The formulation and preparation of stearic acid SLNs was optimized to enable encapsulation of BpT and Bp4eT. The lipid concentration, drug : lipid molar ratio and concentration of surfactant are known to have significant influences on the particle size and drug entrapment efficiency. The effects of various processing parameters, such as the lipid : drug ratio, surfactant ratio (soya lecithin : Tween 80) and volume of aqueous and organic phases were optimized to obtain a good combination of small particle size (low PDI) and high entrapment efficiency to yield effective BpT and Bp4eT loaded SLN formulations.

Physicochemical properties are vital across all possible applications of SLNs. The effect of using various materials (lipid, surfactants, polymer conjugated targeting ligand) and preparation methods on the characteristics and properties of the developed SLNs were all taken into account to examine the particle size, zeta potential, morphology and thermal properties of these targeted SLN formulations.⁴⁴ The mean particle size distributions of BpT-PB-SLNs and Bp4eT-PB-SLNs were obtained as 117.6 nm (PDI 0.169) and 124.8 nm (PDI 0.048), respectively (Fig. 1). The PDI values of less than 0.3 indicated the homogeneity of the nanoformulations. The zeta potentials of BpT-PB-SLNs and Bp4eT-PB-SLNs were found to be -28.5 and -33.3 mV, respectively, indicating the stability of these nanoformulations, as absolute zeta potential values around 25 mV are known to favour storage stability.⁴⁵

The loading of iron chelators (BpT and Bp4eT) in the SLN nanocarriers was verified by UV-Vis spectrophotometry. Both BpT and its analogue showed a slight red shift from 330 nm to 340 nm on encapsulation into the SLNs, which confirmed the

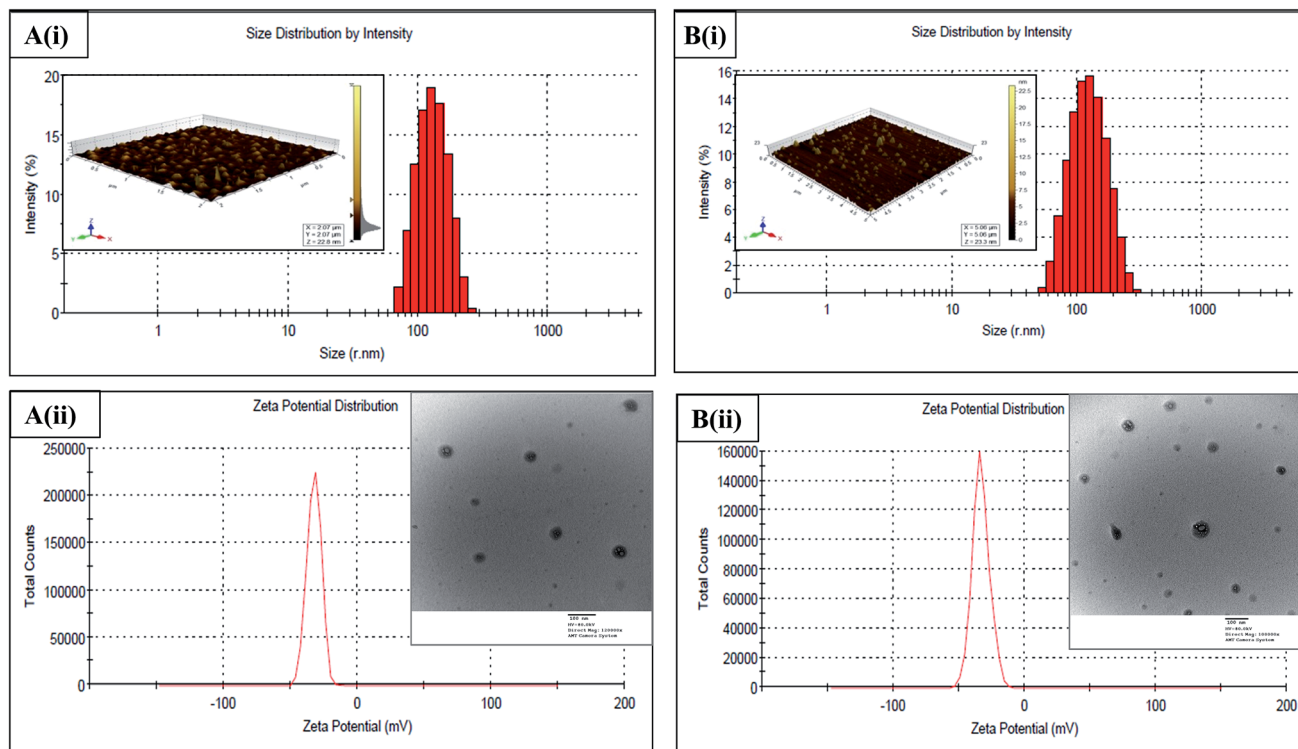


Fig. 1 Size distribution of BpT-PB-SLNs (A(i)) and Bp4eT-PB-SLNs (B(ii)) by DLS. Insets show their respective morphology by AFM. Zeta potential of BpT-PB-SLNs (A(ii)) and Bp4eT-PB-SLNs (B(ii)). Insets show their respective TEM images.

encapsulation of the drugs in the nanocarrier systems (Fig. 2). The encapsulation efficiencies of BpT and Bp4eT in BpT-PB-SLNs and Bp4eT-PB-SLNs are 70% and 72%, respectively, and the drug loadings of the respective systems were around 20 and 22%. The chemical and physical structure of the solid lipid matrix, the solubility of drug in melted lipid, the miscibility of the drug melt and the lipid melt, and the polymorphic state of the lipid material are certain factors which govern the encapsulation efficiency and loading capacity of an SLN formulation. Of these, high solubility of the drug in the lipid melt is a prerequisite to achieve good loading capacity.³¹ In the present case, the hydrophobic nature of these iron chelators, BpT and Bp4eT, and their good solubility in the lipid melt (tried experimentally up to a 1 : 1 ratio) could facilitate

a maximum encapsulation efficiency of up to 72% and a loading content of around 25%, which is a high value when considering that SLNs are known to show lower drug loadings than their liposomal counterparts.⁴⁶ However, their biocompatible compositions and the ability to remain in a solid state at physiological temperatures gives them an advantage over liposomes.

The TEM micrographs revealed the spherical surface morphology of these nanoformulations. The TEM images show a dark core of the particles, clearly depicting the drug loading in the core of the SLNs (Fig. 1). Images acquired by the very tiny AFM tip, after immobilization of the SLNs on the silicon wafers, also validated this finding (Fig. 1).

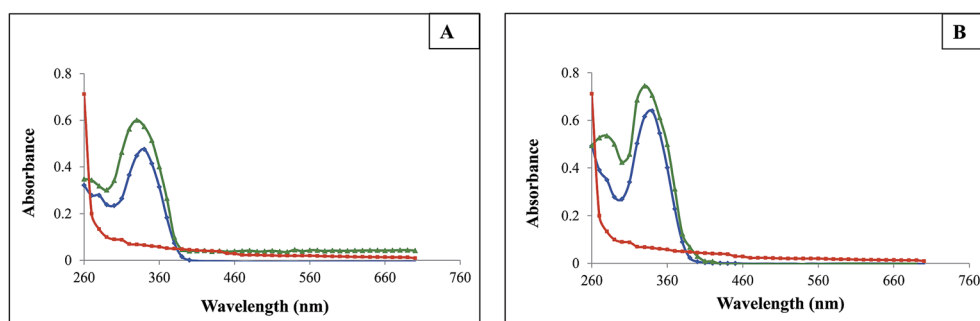


Fig. 2 UV-Vis spectra depicting red shift on drug loading in BpT-PB-SLNs (A) and Bp4eT-PB-SLNs (B). — PSS, — BpT, — BpT-PB-SLNs, — Bp4eT, — Bp4eT-PB-SLNs.

Drug release – kinetics discussion

In vitro release studies under simulated physiological conditions are essential to comprehend the effect of a drug. For this, it is essential to realize in what form and to what extent the drug is encapsulated in a carrier system. Generally, the drug molecules are not only loaded in the core of the lipid matrix but also become entrapped in the outer shell of the lipid matrix.⁴⁷ To evaluate the extent and form of drugs encapsulated in these biotinylated solid lipid nanoparticles, the *in vitro* release profile was constructed in the form of the percentage of drug (BpT and Bp4eT) released from the SLNs cumulatively as a function of time. Fig. 3 profiles the drug release at two pH values: pH 7.4 to simulate the physiological environment, and pH 5.5 to simulate the acidic tumour microenvironment. In the case of Bp4eT-PB-SLNs, almost 14% and 23% of the drug was released in the first 24 h at pH 5.5 and 7.4, respectively. A possible explanation is that the drugs must travel a longer diffusion path due to enrichment of the drug in the core of the SLN rather than being loosely bound in the outer shell of the lipid matrix; hence, no burst release was observed. Such an enrichment might occur due to the solidification of the SLN during the quenching of the lipids during mixing of the organic and aqueous phases. This quenching could also have avoided the heterogeneous crystallization of the drugs owing to the distinctly higher melting point of the drug (151 to 153 °C) than the lipid (~55 °C). Subsequently, there was a very slow rate of release after 24 h. Only 7 to 10% of the drug was released over the next 7 days, and the maximum release went up to 21% and 32.5% respectively, until day 7. Nonetheless, the release profiles had an increasing trend, indicating that further release can be expected with increasing time duration. This clearly demonstrates a highly sustained release system that initially releases part of the dose contained in it, in order to rapidly attain the effective therapeutic concentration of the drug. Thereafter, the drug release kinetics follows a well-defined behavior in order to supply the maintenance dose, enabling the attainment of the desired drug concentration. As expected, the solid state of the lipids in the SLNs prolonged the release of the entrapped drugs from the nanoparticles. These results validate the possibility of a controlled release from SLNs, as also reported in an earlier study.⁴⁸

Release kinetics

Controlled release systems have versatile applications and are therefore becoming imminent research aids for therapeutic treatment. In this scenario, the use of mathematical modeling has been found to be a very useful tool in the prediction of release kinetics before the drug loaded systems are realized, as they allow the measurement of some important physical parameters, such as the drug diffusion coefficient, and resort to model fitting on experimental release data.⁴⁹ The experimental data obtained from the *in vitro* drug release studies of BpT-PB-SLNs and Bp4eT-PB-SLNs was modeled according to different release kinetic models such as zero order, first order, Higuchi and Korsmeyer–Peppas (Power law) models to authenticate the mechanism of release. Of these models, the release profiles gave a better fit to the Korsmeyer–Peppas model, as evident from the high values of the correlation coefficient, r^2 (Fig. 3). Since the spherical shape of the SLNs was validated from the TEM images, the values of the power law exponent, n , for a sphere have been used. The model fitting revealed a Fickian release mechanism at pH 7.4 with $n = 0.2$ ($n < 0.43$) and a non-Fickian transport at acidic pH 5.5 with $n = 0.62$ ($0.43 < n < 0.89$). Drug release by the Fickian diffusion has been found to be generally true irrespective of the method of production, and this was correlated with the legitimate use of the Korsmeyer–Peppas model to describe Fickian diffusion from lipid matrices, as has been reported.

In vitro evaluation

Hemolysis. For formulations intended to be administered by the intravenous route, it is imperative to determine their toxicity in blood; evaluation of hemolytic activity is the best method to accomplish this. This study became all the more relevant when patients undergoing phase I and II clinical trials with Triapine were reported to show severe methaemoglobinemia and hemolysis after treatment.⁵⁰ The basic objective of this study was to quantify the damaging effects of BpT-PB-SLNs and Bp4eT-PB-SLNs on the RBC membrane. 2% Triton X-100 and Phosphate Buffer Saline 7.4 (PBS 7.4) were used as the positive and negative controls for this study. Erythrocytes were incubated at 37 °C with BpT-PB-SLN and Bp4eT-PB-SLN samples; any RBC lysis was estimated from the absorbance of the sample measured, post centrifugation, at 540 nm. It was found that even up to 4 h, BpT-

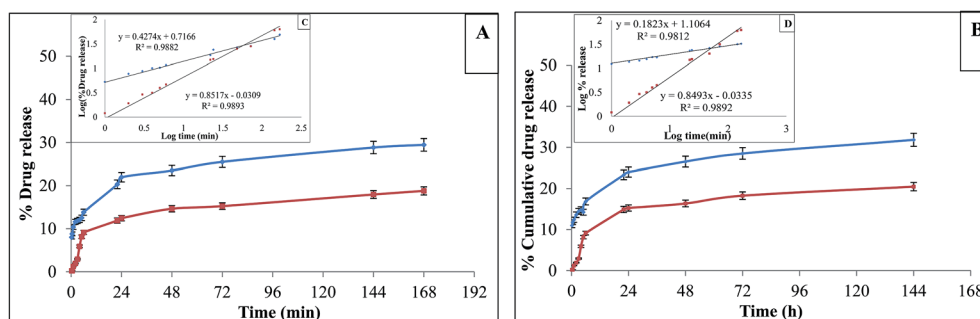


Fig. 3 *In vitro* drug release of BpT-PB-SLNs (A) and Bp4eT-PB-SLNs (B) at pH values 5.5 and 7.4. (C) and (D) show the Korsmeyer–Peppas models respectively. —●— BpT release @ pH 5.5, —●— BpT release @ pH 7.4, —●— Bp4eT release @ pH 5.5, —●— Bp4eT release @ pH 7.4.

PB-SLNs and Bp4eT-PB-SLNs showed only 0.45% and 0.49% hemolytic activity with respect to the negative control, as also exemplified by the sample images (Fig. 4). These values were well within the biologically acceptable range of 5% as per ASTM standards. This study therefore indicated that BpT-PB-SLNs and Bp4eT-PB-SLNs are completely safe to erythrocytes and are suitable for the intravenous mode of injection.

Methemoglobin formation. Methemoglobin formation, an important side effect of using iron chelators such as BpT and Bp4eT, was evaluated when iron complexes of BpT and Bp4eT and their SLN loaded formations were incubated with RBC lysates at 37 °C. The activity of BpT and Bp4eT-iron complexes showed an increasing formation of methemoglobin as a function of time. Almost a 4-fold increase was observed for these iron chelators relative to DFO at 1 h post incubation, which increased to almost 20-fold over a 4 h period (Fig. 5). Almost negligible methemoglobin formation was observed in the case of the nanoparticle-packaged chelators, thus demonstrating that nanoparticle-packaging aids in preventing methemoglobin formation by the encapsulated iron chelators, thus ensuring that these BpT-PB-SLNs and Bp4eT-PB-SLNs are less prone to generate methemoglobin *in vivo*.

Cell viability. After the evaluation of blood toxicity, the cytotoxicity of BpT-PB-SLNs and Bp4eT-PB-SLNs was determined using the SRB assay on healthy non-tumour cells human embryonic kidney cells (HEK cells). The sulforhodamine B assay was chosen over the MTT assay to estimate the *in vitro* cytotoxicity of the SLNs because of its sensitivity to the function of mitochondria, which are also sensitive to iron chelators. The

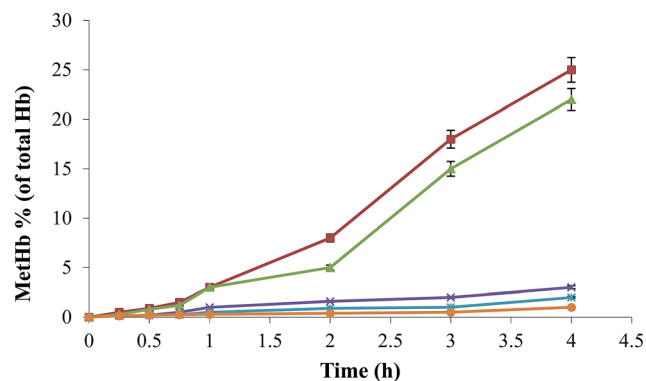


Fig. 5 Methemoglobin formation test of BpT and Bp4eT in RBC lysates. —○— DFO, —▲— BpT, —■— Bp4eT, —×— BpT-PB-SLNs, —*— Bp4eT-PB-SLNs.

continuous form of the protocol was applied to the test, and the data obtained were used to calculate the viability percentage; this has been plotted in Fig. 6. At the end of 12 h, BpT and Bp4eT were found to inhibit 50% of the HEK cells at 2 μM and 2.5 μM concentrations, respectively. In contrast, the BpT-PB-SLNs and Bp4eT-PB-SLNs showed almost negligible inhibition, even up to the 48 h time point. After the cell viability assessment, these drug loaded nano-formulations were then chosen for further *in vivo* evaluations.

Radiolabeling and *in vivo* evaluation: kinetics, biodistribution, SPECT imaging

Pharmacokinetic evaluations of the iron chelator loaded SLN formulations were facilitated by radiolabeling them with technetium-99m radionuclide to obtain the whole body *ex vivo* distribution and the *in vivo* image of these formulations.⁴⁹ Both BpT-PB-SLNs and Bp4eT-PB-SLNs were labeled with ^{99m}Tc by the direct labeling method with high reproducible labeling efficiency. All the labeling parameters with respect to pH, stannous chloride concentration, temperature and incubation time were duly optimized so as to obtain the maximum labeling efficiency and the minimum percentage of reduced and

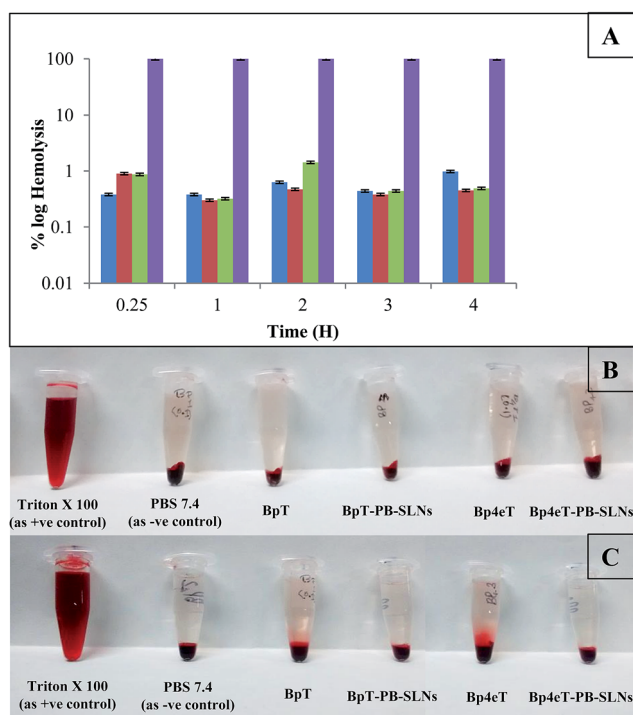


Fig. 4 Hemolysis plot of BpT-SLNs and Bp4eT-SLNs (A). (B) and (C) show images 1 h and 4 h respectively. —■— Triton, —■— PBS 7.4, —■— BpT-BP-SLNs, —■— Bp4eT-PB-SLNs.

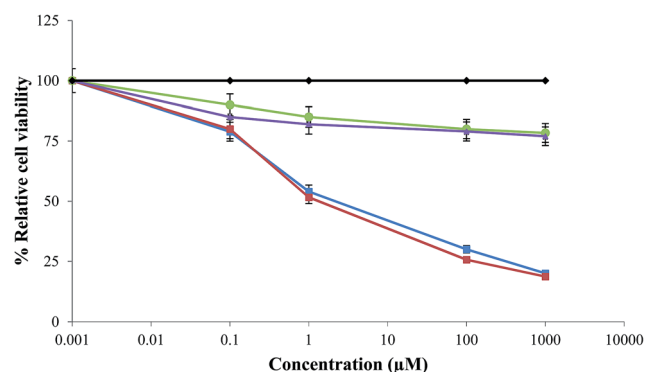


Fig. 6 SRB assay of BpT-PB-SLNs and Bp4eT-PB-SLNs in HEK cells. —◆— Control, —■— BpT, —■— Bp4eT, —●— BpT-PB-SLNs, —▲— Bp4eT-PB-SLNs.

hydrolyzed colloids (Fig. S8†). We were able to achieve a labeling efficiency of >99% for both the formulations, and they were found to remain stable (>98% efficiency) up to 24 h in serum in a reproducible manner without much proteolytic degradation (Fig. S9†). These radiolabeled formulations, ^{99m}Tc -BpT-PB-SLN and ^{99m}Tc -Bp4eT-PB-SLN, were then used for the blood kinetics, biodistribution and scintigraphic analysis.

Blood kinetics

To evaluate the post injection retention time of these iron chelators in blood circulation, blood kinetics studies were performed.⁵⁰ New Zealand albino rabbits were used for this study, as they provide a sufficient quantity of blood for *ex vivo* evaluation at different time points. Intravenous injection of 300 μL of ^{99m}Tc -labelled BpT-PB-SLNs and Bp4eT-PB-SLNs in rabbits revealed slow and biphasic clearance of these compounds from blood circulation compared to the relatively faster clearance of the ^{99m}Tc labeled native drugs, BpT and Bp4eT, as shown in the semilogarithmic plot representing the amount of radioactivity remaining in the blood with the passage of time (Fig. 7). This plot showed that our system follows the 'Two-compartment open model', in which one central compartment comprises the highly perfused tissue/organs and the other compartment comprises the less perfused tissues/organs; this was further used to calculate the half-lives of intact and encapsulated chelators. It was further deciphered that after 4 h post injection (p.i.), only 2.8% and 4.5% of the injected ^{99m}Tc -BpT and ^{99m}Tc -Bp4eT remained in circulation; these were reduced to 0.69% and 1%, respectively, 24 h p.i. Contrastingly, almost 16.5% of the ^{99m}Tc -BpT-PB-SLNs and 19% of the injected ^{99m}Tc -Bp4eT-PB-SLNs were retained in systemic circulation 4 h p.i., and significant amounts of 12% and 10% of the injected ^{99m}Tc -BpT-PB-SLNs and ^{99m}Tc -Bp4eT-PB-SLNs, respectively, were found in the blood circulation even 24 h p.i. The half-life of ^{99m}Tc -BpT was determined to be 30 min ($t_{1/2}$ fast) and 6 h 15 min ($t_{1/2}$ slow), whilst that of ^{99m}Tc -Bp4eT were found to be 35 min ($t_{1/2}$ fast) and 10 h ($t_{1/2}$ slow). The half-life of ^{99m}Tc -BpT-PB-SLNs was found to be 50 min ($t_{1/2}$ fast) and 24 h 30 min ($t_{1/2}$ slow), while that of ^{99m}Tc -Bp4eT-PB-SLNs was found to be 1 h 15 min ($t_{1/2}$ fast) and 26 h ($t_{1/2}$ slow). The blood kinetics studies using these

^{99m}Tc -labeled SLN formulations illustrated the higher retention time of the iron chelators post encapsulation into SLNs than in the native state. High blood retention increases the probability of their retention in the tumour microenvironment and therefore enhances the scope of uptake of these iron chelators by tumour cells (owing to their encapsulation in SLNs), facilitated by the leaky lymphatic system of tumour tissues, which prevents the drainage of these nanocarriers.⁵¹ This is in contrast to conventional drugs, which have low retention in the tissues/organs of interest owing to the active lymphatic system in normal cells.

The stability of the ^{99m}Tc -labelled BpT-PB-SLNs and Bp4eT-PB-SLNs was studied in human serum for up to 24 h. From Fig. S9,† it can be predicted that the two complexes will be extremely stable in the *in vivo* environment (human serum) with a labeling efficiency of >98%.

Biodistribution studies

The results obtained after the biodistribution study of the radiolabelled BpT-PB-SLNs and Bp4eT-PB-SLNs are shown in Fig. 8, wherein the percentage of the injected dose taken up by various organs at different time points has been given. The pre-targeting protocol involved prior administration of avidin to establish secondary binding sites on the tumour that could be more efficiently targeted by the biotinylated formulations. Both the labeled compounds, ^{99m}Tc BpT-PB-SLNs and Bp4eT-PB-SLNs, exhibited high initial radioactivity in the lungs, kidneys and blood, whereas the intact ^{99m}Tc -BpT and ^{99m}Tc -Bp4eT showed high radioactivity in the lungs, intestine, liver and blood at the initial time points. The higher radioactivity of ^{99m}Tc -BpT and ^{99m}Tc -Bp4eT in the intestines and liver may be attributed to their lipophilic character; however, in the encapsulated form, they primarily showed a renal route of excretion (Fig. S10† shows the biodistribution profile of ^{99m}Tc -BpT and ^{99m}Tc -Bp4eT).²¹ A significantly high accumulation of activity in the liver and kidneys (1.94% ID and 7.5% ID of BpT-PB-SLNs, 3.088% ID and 8.78% ID of Bp4eT-PB-SLNs after 2 h and 2.75% ID and 7.23% ID of BpT-PB-SLNs, 2.73% ID and 9.48% ID of Bp4eT-PB-SLNs after 4 h of injection of the labeled complexes) indicated their hepatobiliary and renal route of clearance from the body. The levels of activity in the spleen were 2.36% ID of BpT-PB-SLNs and 3.94% ID of Bp4eT-PB-SLNs after 2 h, and 1.76% ID of BpT-PB-SLNs and 1.56% ID of Bp4eT-PB-SLNs after 4 h post-injection, while a high level of activity was found in the lungs (5.3% ID of BpT-PB-SLNs and 5.29% ID of Bp4eT-PB-SLNs after 2 h and 6.01% ID of BpT-PB-SLNs and 7.2% ID of Bp4eT-PB-SLNs after 4 h post-injection). Quantitative uptake of the nanoformulations was found in the tumour to the extent of 3.5% and 4.8% of the injected dose for BpT-PB-SLNs and Bp4eT-PB-SLNs, respectively (at 4 h p.i.); these values continued to increase with increasing time. This was in correlation with the high anti-tumour activity of the BpT class of chelators demonstrated against human DMS-53 lung xenografts in nude mice.¹⁹ The target to non-target ratio was calculated at different time points in the study in the form of tumour uptake *versus* uptake in the normal contralateral side (Fig. 8). The ratio

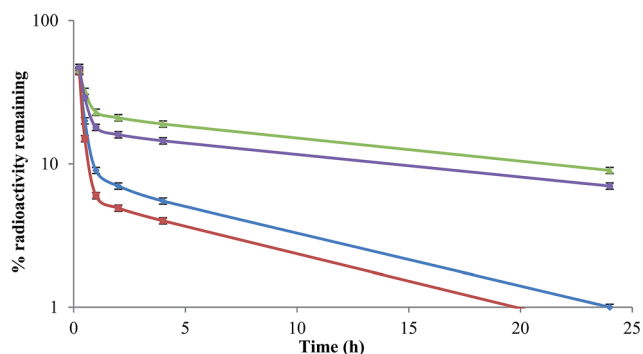


Fig. 7 Logarithmic plot of blood kinetics of BpT-PB-SLNs and Bp4eT-PB-SLNs in New Zealand albino rabbits. —■— BpT, —◆— Bp4eT, —●— BpT-PB-SLNs, —▲— Bp4eT-PB-SLNs.

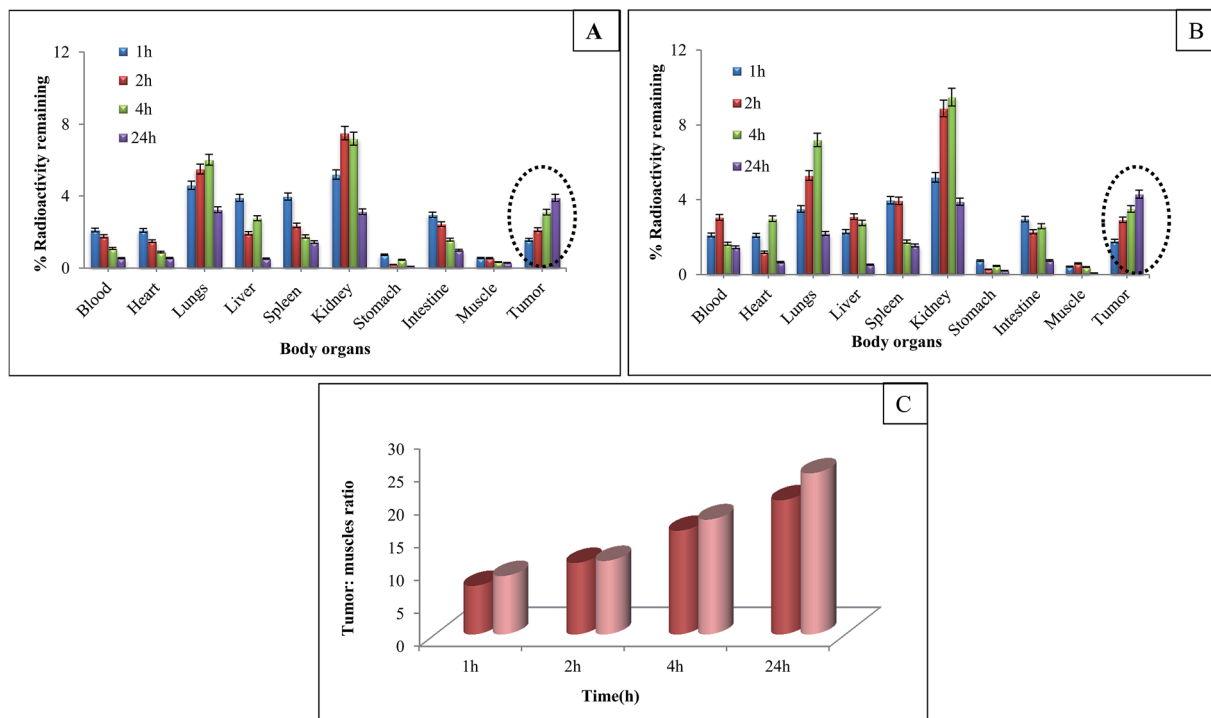


Fig. 8 Biodistribution of BpT-PB-SLNs (A) and Bp4eT-PB-SLNs (B) at 1 h, 2 h, 4 h and 24 h. (C) Tumour : muscle distribution at different time intervals. ■ BpT-PB-SLNs, ■ Bp 4eT-PB-SLNs.

was highest at the 4 h time point and showed an increasing trend even at the 24 h time point, perhaps owing to the retention of these formulations at the tumour site, whilst the labeled compounds continued to be eliminated from the other tissues and organs due to the decreased retention. This uptake was significantly blocked (by >90%) in animals receiving a high dose of avidin together with the radiolabeled formulations, as expected. These biodistribution studies proved the higher systemic circulation of this system, as exemplified by the persistence of BpT-SLNs and Bp4eT-SLNs in tumour tissue for up to 24 h.

Scintigraphy in tumour-bearing mice

Scintigraphic imaging was performed in A-549 xenografted athymic mice following intravenous administration of the radiolabeled formulations, ^{99m}Tc -BpT-PB-SLNs and ^{99m}Tc -Bp4eT-PB-SLNs, co-injected with avidin. High uptake of the biotinylated SLN formulations was seen at the tumour site, which was quantified by semiquantitative analysis of the region of interest (ROI) placed over the tumour region quantifying the average counts per pixel with respect to the whole body uptake. The ratio of tumour uptake to the whole body was found to be almost 11% compared to the uptake by the rest of the body. The biotin-avidin binding was validated by this gamma imaging, which gave us a clear visual demonstration of the uptake of these radiolabeled formulations in the tumour regions of the xenografted mice. Images of the mice were taken at different time points, showing the beginning of the accumulation of the complexes in the tumour sites after 1 h, which later reached

a maximum after 4 h and then remained stable. When compared with the uptake in the contralateral muscle, the tumour-to-muscle ratios were found to be 15.8 and 20.4 for BpT-

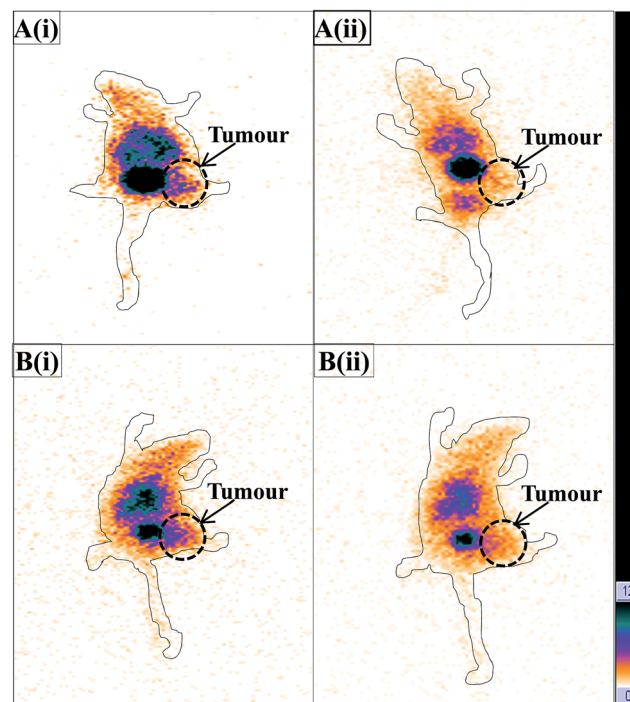


Fig. 9 SPECT images of BpT-PB-SLNs (A(i)) Bp4eT-PB-SLNs (B(i)) and those with biotin challenge (A(ii) and B(ii) respectively).

PB-SLNs and 18.3 and 24.29 for Bp4eT-PB-SLNs after 4 h and 24 h, respectively (Fig. 9).

Scintigraphic whole body imaging of the A549 tumour xenografted athymic mice correlated well with the biodistribution studies. These preliminary preclinical results demonstrated a promising future for these novel SLN formulations encapsulating BpT and Bp4eT iron chelators, particularly for A549 tumours, to help achieve lower intracellular Fe concentrations and thus limit cell proliferation.

Conclusions

To summarize, novel nanoformulations based on biotin functionalized SLNs have been developed from synthesized iron chelators, BpT and Bp4eT. The formulations, with average hydrodynamic sizes around 120 nm, were evaluated for their hemolytic activity, pharmacokinetics and tumour uptake and were found to show good tumour retention and negligible RBC toxicity. A pragmatic approach to use two-step pretargeting has shown encouraging initial results to achieve high tumour uptake of these iron chelators with low non-specific retention in the physiological environment. The results generated in this work indicate that these BpT/Bp4eT loaded biotin-functionalized SLNs are potential candidates to be used as biocompatible nanocarrier systems with high systemic retention and anti-tumour effects.

Acknowledgements

This work has been carried out under project INM-311(3.1). We thank Dr A. K. Singh, Director INMAS, for providing necessary facilities and infrastructure for carrying out this research work. Financial assistance provided to SD by CSIR, India, is duly acknowledged. We are thankful to SSPL, DRDO and the USIC facility of Delhi University for instrumentation support.

References

- 1 S. Guo and L. Huang, Nanoparticles Escaping RES and Endosome: Challenges for siRNA Delivery for Cancer Therapy, *J. Nanomater.*, 2011, **2011**, 12.
- 2 K. Kobayashi, J. Wei, R. Iida, K. Ijio and K. Niikura, Surface engineering of nanoparticles for therapeutic applications, *Polym. J.*, 2014, **46**, 460–468.
- 3 M. J. Akhtar, M. Ahamed, H. A. Alhadlaq, S. A. Alrokayan and S. Kumar, Targeted anticancer therapy: overexpressed receptors and nanotechnology, *Clin. Chim. Acta*, 2014, **436**, 78–92.
- 4 M. Vanneman and G. Dranoff, Combining immunotherapy and targeted therapies in cancer treatment, *Nat. Rev. Cancer*, 2012, **12**, 237–251.
- 5 R. Baskar, K. A. Lee, R. Yeo and K. W. Yeoh, Cancer and Radiation Therapy: Current Advances and Future Directions, *Int. J. Med. Sci.*, 2012, **9**, 193–199.
- 6 J. L. Heath, J. M. Weiss, C. P. Lavau and D. S. Wechsler, Iron Deprivation in Cancer-Potential Therapeutic Implications, *Nutrients*, 2013, **5**, 2836–2859.
- 7 T. R. Daniels, E. Bernabeu, J. A. Rodríguez, S. Patel, M. Kozman, D. A. Chiappetta, E. Holler, J. Y. Ljubimova, G. Helguera and M. L. Penichet, The transferrin receptor and the targeted delivery of therapeutic agents against cancer, *Biochim. Biophys. Acta*, 2012, **1820**, 291–317.
- 8 J. Yuan, D. B. Lovejoy and D. R. Richardson, Novel di-2-pyridyl-derived iron chelators with marked and selective antitumor activity: *in vitro* and *in vivo* assessment, *Blood*, 2004, **104**, 1450–1458.
- 9 J. Blatt and S. Stitley, Antineuroblastoma activity of desferoxamine in human cell lines, *Cancer Res.*, 1987, **47**, 1749–1750.
- 10 T. Yamasaki, I. Saeki and I. Sakaida, Efficacy of iron chelator desferoxamine for hepatic arterial infusion chemotherapy in advanced hepatocellular carcinoma patients refractory to current treatments, *Hepatol. Int.*, 2014, **8**, 492–498.
- 11 J. Turner, C. Koumenis, T. E. Kute, R. P. Planalp, M. W. Brechbiel, D. Beardsley, B. Cody, K. D. Brown, F. M. Torti and S. V. Torti, Tachpyridine, a metal chelator, induces G2 cell-cycle arrest, activates checkpoint kinases, and sensitizes cells to ionizing radiation, *Blood*, 2005, **106**, 3191–3199.
- 12 J. Gao and D. R. Richardson, The potential of iron chelators of the pyridoxal isonicotinoylhydrazone class as effective antiproliferative agents, IV: the mechanisms involved in inhibiting cell-cycle progression, *Blood*, 2001, **98**, 842–850.
- 13 A. M. Merlot, N. Pantarat, D. B. Lovejoy, D. S. Kalinowski and D. R. Richardson, Membrane Transport and Intracellular Sequestration of Novel Thiosemicarbazone Chelators for the Treatment of Cancer, *Mol. Pharmacol.*, 2010, **78**, 675–684.
- 14 Y. Yu, Y. S. Rahmanto and D. R. Richardson, Bp44mT: an orally active iron chelator of the thiosemicarbazone class with potent anti-tumour efficacy, *Br. J. Pharmacol.*, 2012, **65**, 148–166.
- 15 D. R. Richardson, D. S. Kalinowski, S. Lau, P. J. Jansson and D. B. Lovejoy, Cancer cell iron metabolism and the development of potent iron chelators as anti-tumour agents, *Biochim. Biophys. Acta*, 2009, **1790**, 702–717.
- 16 P. N. Dayani, M. C. Bishop, K. Black and P. M. Zeltzer, Desferoxamine (DFO) – Mediated Iron Chelation: Rationale for a Novel Approach to Therapy for Brain Cancer, *J. Neuro-Oncol.*, 2004, **67**, 367–377.
- 17 J. J. Knox, S. J. Hotte, C. Kollamannsberger, E. Winquist, B. Fisher and E. A. Eisenhauer, Phase II study of Triapine® in patients with metastatic renal cell carcinoma: a trial of the National Cancer Institute of Canada Clinical Trials Group (NCIC IND.161), *Invert New Drugs*, 2007, **25**, 471–477.
- 18 I. Gojo, M. L. Tidwell, J. Greer, N. Takebe, K. Seiter, M. F. Pochron, B. Johnson, M. Sznol and J. E. Karp, Phase I and pharmacokinetic study of triapine, a potent ribonucleotide reductase inhibitor, in adults with advanced hematologic malignancies, *Leuk. Res.*, 2007, **31**, 1165–1173.
- 19 M. Whitnall, J. Howard, P. Ponka and D. R. Richardson, A class of iron chelators with a wide spectrum of potent antitumor activity that overcomes resistance to

- chemotherapeutics, *Proc. Natl. Acad. Sci. U. S. A.*, 2006, **103**, 14901–14906.
- 20 A. M. Merlot, S. Sahni, D. J. Lane, A. M. Fordham, N. Pantarat, D. E. Hibbs, D. E. Richardson, M. R. Doddareddy, M. L. Huang, D. R. Richardson and D. S. Kalinowski, Potentiating the cellular targeting and anti-tumor activity of Dp44mT *via* binding to human serum albumin: two saturable mechanisms of Dp44mT uptake by cells, *Oncotarget*, 2015, **6**, 10374–10398.
- 21 M. Merlot, N. Pantarat, S. V. Menezes, S. Sahni, D. R. Richardson and D. S. Kalinowski, Cellular uptake of the antitumor agent Dp44mT occurs *via* a carrier/receptor-mediated mechanism, *Mol. Pharmacol.*, 2013, **84**, 911–924.
- 22 J. Stariat, V. Suprunova, J. Roh, V. Sestak, T. Eisner, T. Filipisky, P. Mladenka, M. Nobilis, T. Simunek, J. Klimes, D. S. Kalinowski, D. R. Richardson and P. Kovarikova, Simultaneous determination of the novel thiosemicarbazone anti-cancer agent, Bp4eT, and its main phase I metabolites in plasma: application to a pilot pharmacokinetic study in rats, *Biomed. Chromatogr.*, 2014, **28**, 621–629.
- 23 Z. Debebe, S. Nekhai, M. Ashenafi, D. B. Lovejoy, D. S. Kalinowski, V. R. Gordeuk, W. M. Byrnes, D. R. Richardson and P. K. Karla, Development of a sensitive HPLC method to measure *in vitro* permeability of E- and Z-isomeric forms of thiosemicarbazones in Caco-2 monolayers, *J. Chromatogr. B: Anal. Technol. Biomed. Life Sci.*, 2012, **1**, 25–32.
- 24 J. Stariat, V. Sestak, K. Vavrova, M. Nobilis, Z. Kollarova, J. Klimes, D. S. Kalinowski, D. R. Richardson and P. Kovarikova, LC-MS/MS identification of the principal *in vitro* and *in vivo* phase I metabolites of the novel thiosemicarbazone anti-cancer drug, Bp4eT, *Anal. Bioanal. Chem.*, 2012, **403**, 309–321.
- 25 A. Kumari, R. Singla, A. Guliani and S. K. Yadav, Nanoencapsulation for drug delivery, *EXCLI Journal*, 2014, **13**, 265–286.
- 26 J. M. Harris and R. B. Chess, Effect of pegylation on pharmaceuticals, *Nat. Rev. Drug Discovery*, 2003, **2**, 214–221.
- 27 J. M. Domi and N. Vera, Iron(III) complexation of desferrioxamine B encapsulated in apoferritin, *J. Inorg. Biochem.*, 2004, **98**, 469–472.
- 28 G. Rassu, A. Salis, E. P. Porcu, P. Giunchedi, M. Roldo and E. Gavini, Composite chitosan/alginate hydrogel for controlled release of deferoxamine: a system to potentially treat iron dysregulation diseases, *Carbohydr. Polym.*, 2016, **136**, 1338–1347.
- 29 Q. Miao, D. Xu, Z. Wang, Y. Wu, D. B. Lovejoy, D. S. Kalinowski, D. R. Richardson, G. Nie and Y. Zhao, Amphiphilic hyper-branched co-polymer nanoparticles for the controlled delivery of anti-tumor agents, *Biomaterials*, 2010, **31**, 7364–7375.
- 30 M. Mir and P. Ebrahimnejad, Preparation and Characterization of Bifunctional Nanoparticles of Vitamin E TPGS-Emulsified PLGA-PEG-FOL Containing Deferasirox, *Nanosci. Nanotechnol.-Asia*, 2014, **4**, 80–87.
- 31 D. K. Thukral, S. Dumoga and A. K. Mishra, Solid Lipid Nanoparticles: Promising Therapeutic Nanocarriers for Drug Delivery, *Curr. Drug Delivery*, 2014, **11**, 771–791.
- 32 D. S. Kalinowski, Y. Yu, P. C. Sharpe, M. Islam, Y. T. Liao, D. B. Lovejoy, N. Kumar, P. V. Bernhardt and D. R. Richardson, Design, synthesis, and characterization of novel iron chelators: structure–activity relationships of the 2-benzoylpyridine thiosemicarbazone series and their 3-nitrobenzoyl analogues as potent antitumor agents, *J. Med. Chem.*, 2007, **50**, 3716–3729.
- 33 J. E. Thomson, C. D. Campbell, C. Concellon, N. Duguet, K. Rix, A. M. Slawin and A. D. Smith, Probing the efficiency of N-heterocyclic carbene promoted O- to C-carboxyl transfer of oxazolyl carbonates, *J. Org. Chem.*, 2008, **73**, 2784–2791.
- 34 D. Kakkar, S. Dumoga, R. Kumar, K. Chuttani and A. K. Mishra, PEGylated solid lipid nanoparticles: design, methotrexate loading and biological evaluation in animal models, *MedChemComm*, 2015, **6**, 1452–1463.
- 35 Standard Practice for Assessment of Hemolytic Properties of Materials, Annual Book of ASTM Standards, Section 13, Medical devices and services, 1998.
- 36 P. Quach, E. Gutierrez, M. T. Basha, D. S. Kalinowski, P. C. Sharpe, D. B. Lovejoy, P. V. Bernhardt, P. J. Jansson and D. R. Richardson, Methemoglobin formation by triapine, di-2-pyridylketone-4,4-dimethyl-3-thiosemicarbazone (Dp44mT), and other anticancer thiosemicarbazones: identification of novel thiosemicarbazones and therapeutics that prevent this effect, *Mol. Pharmacol.*, 2012, **82**, 105–114.
- 37 D. R. Richardson, P. C. Sharpe, D. B. Lovejoy, D. Senaratne, D. S. Kalinowski, M. Islam and P. V. Bernhardt, Dipyrindyl Thiosemicarbazone Chelators with Potent and Selective Antitumor Activity Form Iron Complexes with Redox Activity, *J. Med. Chem.*, 2006, **49**, 6510–6521.
- 38 D. Kakkar, A. K. Tiwari, K. Chuttani, R. Kumar, K. Mishra, H. Singh and A. K. Mishra, Pegylated isoniazid conjugate for reduced toxicity and sustained release, *Ther. Delivery*, 2011, **2**, 205–212.
- 39 D. Kakkar, A. K. Tiwari, K. Chuttani, A. Kaul, H. Singh and A. K. Mishra, Comparative Evaluation of Glutamate-Sensitive Radiopharmaceuticals: Technetium-99m–Glutamic Acid and Technetium-99m–Diethylenetriaminepentaacetic Acid–Bis(Glutamate) Conjugate for Tumor Imaging, *Cancer Biother. Radiopharm.*, 2010, **25**, 645–656.
- 40 H. Cabral, Y. Matsumoto, K. Mizuno, Q. Chen, M. Murakami, M. Kimura, Y. Terada, M. R. Kano, K. Miyazono, M. Uesaka, N. Nishiyama and K. Kataoka, Accumulation of sub-100 nm polymeric micelles in poorly permeable tumours depends on size, *Nat. Nanotechnol.*, 2011, **6**, 815–823.
- 41 Y. Xing, L. Liu, D. Zhao, Y. Yang and X. Chu, Synthesis of water-dispersed ferrocene/phenylboronic acid-modified bifunctional gold nanoparticles and the application in biosensing, *Materials*, 2014, **7**, 5554–5564.
- 42 T. Yau, X. Dan, C. C. W. Ng and T. B. Ng, Lectins with potential for anticancer therapy, *Molecules*, 2015, **20**, 3791–3810.

- 43 A. Kevacevic, S. Savic, G. Vuleta, R. H. Muller and C. M. Keck, Polyhydroxy surfactants for the formulations of lipid nanoparticles (SLN and NLCs): effects on size, physical stability and particle matrix structure, *Int. J. Pharm.*, 2011, **406**, 163–172.
- 44 S. Mukherjee, S. Ray and R. S. Thakur, Solid Lipid Nanoparticles: A Modern Formulation Approach in Drug Delivery System, *Indian J. Pharm. Sci.*, 2009, **71**, 349–358.
- 45 R. H. Muller, M. Radtke and S. A. Wissing, Solid lipid nanoparticles (SLN) and nanostructured lipid carriers (NLC) in cosmetic and dermatological preparations, *Adv. Drug Delivery Rev.*, 2002, **54**(suppl. 1), S131–S155.
- 46 A. Z. Muhlen, C. Schwarz and W. Mehner, Solid lipid nanoparticles (SLN) for controlled drug delivery–drug release and release mechanism, *Eur. J. Pharm. Biopharm.*, 1998, **45**, 149–155.
- 47 S. Dash, P. N. Murthy, L. Nath and P. Chowdhary, Kinetic modelling on drug release from controlled drug delivery systems, *Acta Pol. Pharm.*, 2010, **67**, 217–223.
- 48 L. M. Foltz, B. J. Dalal, L. D. Wadsworth, R. Broady, K. Chi, E. Eisenhauer, K. Kobayashi and C. Kollmannsburger, Recognition and management of methemoglobinemia and hemolysis in a GGPD-deficient patient on experimental anticancer drug triapine, *Am. J. Hematol.*, 2006, **81**, 210–211.
- 49 D. Kakkar, A. K. Tiwari, K. Chuttani, A. Khanna, A. Datta, H. Singh and A. K. Mishra, Design, Synthesis and Antimycobacterial Property of PEG-bis(INH) Conjugates, *Chem. Biol. Drug Des.*, 2012, **80**, 245–253.
- 50 D. K. Thukral, S. Dumoga, S. Arora, K. Chuttani and A. K. Mishra, Potential carriers of chemotherapeutic drugs: matrix based nanoparticulate polymeric systems, *Cancer Nanotechnol.*, 2014, **5**, 3.
- 51 M. Uner and G. Yener, Importance of solid lipid nanoparticles (SLN) in various administration routes and future perspectives, *Int. J. Nanomed.*, 2007, **2**, 289–300.